

Massive neutron stars with multiquark cores

Sitthichai Pinkanjanarod^{1, 2, *} and Piyabut Burikham^{1, †}

¹*High Energy Physics Theory Group, Department of Physics,*

Faculty of Science, Chulalongkorn University, Bangkok 10330, Thailand

²*Department of Physics, Faculty of Science, Kasetsart University, Bangkok 10900, Thailand*

(Dated: December 22, 2024)

Phases of nuclear matter are crucial in determination of the physical properties of neutron stars (NS). In the core of NS, it is possible that the density and pressure become so large that the nuclear matter undergoes phase transition into a deconfined phase, consisting of quarks and gluons and their colour bound states. Even though the quark-gluon plasma has been observed in ultra-relativistic heavy-ion collisions[1, 2], it is still unclear whether exotic quark matter exists inside neutron stars. Recently the result from the combination of various perturbative theoretical calculations with astronomical observations[3, 4] shows that (exotic) quark matter could exist inside the cores of neutron stars above 2.0 solar masses (M_{\odot}) [5] However, due to the nonperturbative characteristic of interactions between quarks and gluons in the deconfined phase, perturbative QCD (pQCD) has limitation due to the possibly large coupling of the quark-gluon soup in such dense environment. We revisit the holographic model in Ref. [6, 7] and implement the equation of states (EoS) of multiquark nuclear matter interpolating from the high-density pQCD EoS and matching with the nuclear EoS known at low densities. It is found that the equations of the states of multiquark nuclear phase provide the missing link between the constraints in both high and low energy density regions and give the mass of NS with multiquark core within the observational range. This shows evidence for the exotic multiquark core inside massive neutron stars. The NS with multiquark core at the maximum mass could have masses in the range $2.0 - 2.8M_{\odot}$ and radii $10 - 14$ km.

1. INTRODUCTION

In the final fate, a star collapses under its own gravity when the internal pressure from nuclear fuel is depleted. The quantum pressure of fermions kicks in to rescue. If the mass of the star is below 0.7 solar mass, the degeneracy pressure of neutrons alone would be able to stop the collapse [8, 9]. Effects of repulsive nuclear force help support the neutron star up to higher masses $> 1.4M_{\odot}$. Given the star is more massive than the upper mass limit of the neutron star, it is believed that it would collapse into a black hole eventually. However, there is a possibility that under extreme pressure and density, the quarks within hadrons would become effectively deconfined from the localized hadrons but still confined by gravity within the star. The deconfined phase of quarks could generate larger pressure to sustain even more massive neutron stars or even quark stars.

Even in the deconfined phase, quarks can still form bound states via the remaining Coulomb-like interaction mediated by gluons, the multiquark states. Observations of multiquark candidates such as pentaquark and tetraquark have been accumulated for decades, see e.g. Ref. [10] for the latest report. It is only natural to imagine an abundance of multiquarks in the core of dense stars where the deconfined quarks are extremely compressed tightly close together. Due to the nonperturbative nature of the strong interaction, the difficulty of lattice QCD approach when dealing with finite baryon

density, and a reliability issue of MIT bag as a tool to study the behaviour of the deconfined quarks and gluons in the dense star, it is therefore interesting to use the equation of state of the deconfined nuclear matter from the holographic model as a complementary tool to other conventional approaches to investigate the properties of the dense star [6, 7].

Recent work [5] reveals a potential double-power-law equation of states (EoS) interpolating between low and high density EoS calculated from the Chiral Effective Field Theory (CET) and perturbative QCD. The empirical EoS gives adiabatic index and sound speed characteristic of the quark matter phase, showing evidence of quark core within the NS. In this work, we revisit the holographic model investigated in Ref. [7] and match the EoS of multiquark nuclear matter with the low and high density EoS and demonstrate that it can interpolate well between the two regions. The masses of NS with multiquark core are consistent with current observations, allowing NS with $M > 2M_{\odot}$ with radii around $10 - 12$ km [3, 4]. Depending on the colour states of multiquark, the mass could be as high as $2.2 - 2.8M_{\odot}$, a potential candidate for the object recently found by LIGO/Virgo [11].

This work is organized as the following. Section 2 reviews holographic model studied in Ref. [7] and presents the EoS of multiquark nuclear matter. Section 3 summarizes the EoS from CET and piecewise polytrope used in the interpolation and EoS of the multiquark core in the high density region. Mass-radius diagram, mass-central density relation and thermodynamic properties of NS with multiquark core are explored in Section 4. Section 5 concludes our work.

*Electronic address: quazact@gmail.com, Sitthichai.P@student.chula.ac.th

†Electronic address: piyabut@gmail.com, piyabut.b@chula.ac.th

2. HOLOGRAPHIC MULTIQUARK AND THE EOS

Within the framework of gauge-gravity duality from superstring theories, bound states of quarks in the boundary gauge theory can be described holographically by strings and branes. Mesons can be expressed as a string hanging in the bulk with both ends locating at the boundary of the AdS space[12] while baryons can be represented by Dp-brane wrapped on the S^p with N_c strings attached and extending to the boundary of the bulk space[13, 14]. The gauge theory from the original AdS/CFT duality is still apart from the actual gauge theory described by QCD. The gauge theory from gravity dual that captures most features of QCD is the Sakai-Sugimoto (SS) model[15, 16]. In this model, hadrons naturally exist in the confined phase however, another kind of bound states of quarks can also occur in the deconfined phase at the intermediate temperatures above the deconfinement, the multiquark states [6, 7]. See e.g. Ref. [17] for a concise review of holographic multiquarks.

2.1. Holographic multiquark configuration

The configuration in the SS model consists of D4-brane background and D8/ $\overline{\text{D8}}$ flavor branes. N_c D4-branes provides 4D $\text{SU}(N_c)$ Yang-Mills gauge theory holographically. On the other hand, N_f D8/ N_f $\overline{\text{D8}}$ flavor branes provide a description for confinement/deconfinement phase transition depending on the configuration of the branes. In terms of symmetry, N_f D8/ N_f $\overline{\text{D8}}$ flavor branes poses the global symmetries $\text{U}(N_f)_L$ and $\text{U}(N_f)_R$ which can fully describe $\text{U}(N_f)_L \times \text{U}(N_f)_R$ chiral symmetry breaking when the D8 and $\overline{\text{D8}}$ are connected. At low energy, the classical solution of the field configuration on the gravity side suggests a cigar-like shape for the compactified spatial direction of a confined background. At high temperature, the cylindrically compactified background spacetime with flavor branes in parallel embedding is preferred, therefore the broken chiral symmetry is restored and the corresponding nuclear matter phase becomes deconfined [18].

In the deconfined phase [6], there are 3 possible configurations as shown in Fig. 1: (i) the parallel configuration of both D8-branes and $\overline{\text{D8}}$ representing the χ_S -QGP (chiral symmetric quark-gluon plasma) and (ii) connected D8- $\overline{\text{D8}}$ without sources in the bulk representing the vacuum with broken chiral symmetry. Another stable configuration (iii) is multiquark phase consisting of the connected D8- $\overline{\text{D8}}$ branes with the D4-brane as the baryon vertex submerged and localized in the middle of the D8 and $\overline{\text{D8}}$. The baryon vertex can be attached with radial hanging strings that represent colour charge of the multiquark configuration.

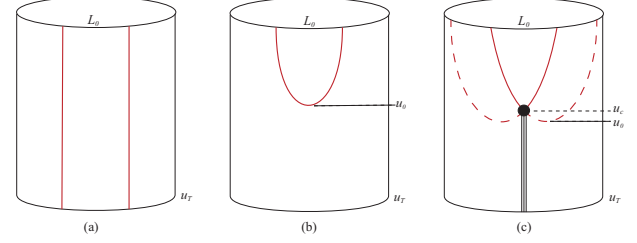


FIG. 1: Different configurations of D8 and $\overline{\text{D8}}$ -branes in the Sakai-Sugimoto model that are dual to the phases of (a) χ_S -QGP, (b) vacuum and (c) multiquark phase. [6]

2.2. Equation of state

Holographically, the grand canonical potential and the chemical potential of the multiquark matter are given by [7]

$$\Omega = \int_{u_c}^{\infty} du \left[1 - \frac{F^2}{f(u)(u^8 + u^3 n^2)} \right]^{-\frac{1}{2}} \frac{u^5}{\sqrt{u^5 + n^2}}, \quad (1)$$

$$\mu = \int_{u_c}^{\infty} du \left[1 - \frac{F^2}{f(u)(u^8 + u^3 n^2)} \right]^{-\frac{1}{2}} \frac{n}{\sqrt{u^5 + n^2}} + \frac{1}{3} u_c \sqrt{f(u_c)} + n_s (u_c - u_T) \quad (2)$$

respectively, where u is a radial coordinate of the background metric of the bulk spacetime in the SS model in a deconfined phase at finite temperature T , $f(u) \equiv 1 - u_T^3/u^3$, $u_T = 16\pi^2 R^3 T^2/9$, $R^3 \equiv \pi g_s N_c l_s^3$, l_s is the string length and g_s is the string coupling. u_c is the position of the baryon vertex source as shown in Fig. 1. n_s is the number fractions of radial strings k_r in the unit of N_c that represents the colour charges of a multiquark configuration. $n(u)$ is the baryon number density which is a constant of the configuration given by

$$n(u) = \frac{u \hat{a}'_0}{\sqrt{f(u)(x'_4)^2 + u^{-3}(1 - (\hat{a}'_0)^2)}} = \text{const.} \quad (3)$$

where x'_4 is the compactified coordinate transverse to the probe D8/ $\overline{\text{D8}}$ branes with arbitrary periodicity $2\pi R$. The $\hat{a} = 2\pi\alpha' \hat{A}/(R\sqrt{2N_f})$ is a rescaled version of \hat{A} , the originally diagonal $U(1)$ gauge field, where α' is a universal Regge slope. The position u_c of the vertex is determined from the equilibrium condition of the D8-D4-strings configuration (see Appendix A of Ref. [6]). Another constant of the configuration is

$$(x'_4)^2 = \frac{1}{u^3 f(u)} \left[\frac{f(u)(u^8 + u^3 n^2)}{F^2} - 1 \right]^{-1} = \text{const.} \quad (4)$$

where F is a function of u_c , n , T and n_s , given by

$$F^2 = u_c^3 f(u_c) \left(u_c^5 + n^2 - \frac{n^2 \eta_c^2}{9 f(u_c)} \right), \quad (5)$$

where $\eta_c \equiv 1 + \frac{1}{2} \left(\frac{u_T}{u_c} \right)^3 + 3n_s \sqrt{f(u_c)}$.

Thermodynamic relations of multiquark states can be found in Ref. [7]. The grand potential G_Ω can be written as

$$dG_\Omega = -PdV - SdT - Nd\mu \quad (6)$$

where the state parameters P , V , S , T , and N are the pressure, volume, entropy, temperature, and the total number of particles of the system respectively. Since the change of volume is not our main concern, we define the volume density of G_Ω , S and N to be Ω , s and n , respectively. Therefore, we have, at a particular T and μ ,

$$P = -G_\Omega/V \equiv -\Omega(T, \mu). \quad (7)$$

Assuming that the multiquark states are spatially uniform, we obtain

$$n = \frac{\partial P}{\partial \mu}(T, \mu). \quad (8)$$

Using the chain rule,

$$\frac{\partial P}{\partial n} \bigg|_T = \frac{\partial \mu}{\partial n} \bigg|_T n, \quad (9)$$

so that

$$P(n, T, n_s) = \mu(n, T, n_s) n - \int_0^n \mu(n', T, n_s) d(n'), \quad (10)$$

where the regulated pressure is assumed to be zero when there is no nuclear matter, i.e. $n = 0$.

2.2.1. Equation of state for multiquark

In the limit of small n , the baryon chemical potential in Eqn.(2) can be approximate as

$$\mu \simeq \mu_{\text{source}} + \alpha_0 n - \beta_0(n_s) n^3, \quad (11)$$

where

$$\begin{aligned} \mu_{\text{source}} &\equiv \frac{1}{3} u_c \sqrt{f(u_c)} + n_s (u_c - u_T) \\ \alpha_0 &\equiv \int_{u_0}^{\infty} du \frac{u^{-5/2}}{1 - \frac{f_0 u_0^8}{f u^8}}, \\ \beta_0(n_s) &\equiv \int_{u_0}^{\infty} du \frac{u^{-5/2}}{2 \sqrt{1 - \frac{f_0 u_0^8}{f u^8}}} \\ &\times \left[\frac{f_0 u_0^3}{f u^8 - f_0 u_0^8} \left(1 - \frac{\eta_0^2}{9 f_0} - \frac{u_0^5}{u^5} \right) + \frac{1}{u^5} \right], \end{aligned}$$

and u_0 is the position when $x'_4(u_0) = \infty$ as shown in Fig. 1.

By substituting Eqn.(11) into Eqn.(10), the pressure in the limit of small n can be expressed as

$$P \simeq \frac{\alpha_0}{2} n^2 - \frac{3\beta_0(n_s)}{4} n^4. \quad (12)$$

In the limit of large n and relatively small T ,

$$\begin{aligned} \mu &\approx \mu_{\text{source}} + \frac{n^{2/5}}{5} \frac{\Gamma(\frac{1}{5}) \Gamma(\frac{3}{10})}{\Gamma(\frac{1}{2})} \\ &+ \frac{u_c^3 f_c}{10} \left(1 - \frac{\eta_c^2}{9 f_c} \right) n^{-4/5} \frac{\Gamma(-\frac{2}{5}) \Gamma(\frac{19}{10})}{\Gamma(\frac{3}{2})} \end{aligned} \quad (13)$$

where the term from lower limit of integration in Eqn.(2), u_c^5/n^2 approaches zero as n becomes very large. Again by using Eqn.(10), we obtain

$$P \simeq \frac{2}{35} \left(\frac{\Gamma(\frac{1}{5}) \Gamma(\frac{3}{10})}{\Gamma(\frac{1}{2})} \right) n^{7/5}. \quad (14)$$

Also the energy density can be found via the relation $d\rho = \mu dn$ and the chemical potential is given by

$$\mu = \int_0^n \frac{1}{\eta} \left(\frac{\partial P}{\partial \eta} \right) d\eta + \mu_0, \quad (15)$$

where $\mu_0 \equiv \mu(n = 0)$. The main results from Ref. [7] are summarized as

$$\begin{aligned} P &= an^2 + bn^4, \\ \rho &= \mu_0 n + an^2 + \frac{b}{3} n^4, \end{aligned} \quad (16)$$

for small n and

$$\begin{aligned} P &= kn^{7/5}, \\ \rho &= \rho_c + \frac{5}{2} P + \mu_c \left[\left(\frac{P}{k} \right)^{5/7} - n_c \right] \\ &+ kn_c^{7/5} - \frac{7k}{2} n_c^{2/5} \left(\frac{P}{k} \right)^{5/7}, \end{aligned} \quad (17)$$

for large n respectively. For $n_s = 0$, $n_c = 0.215443$, $\mu_c = 0.564374$ (core), $a = 1$, $b = 0$, $\mu_0 = 0.17495$ (crust). For $n_s = 0.3$, $n_c = 0.086666$, $\mu_c = 0.490069$ (core), $a = 0.375$, $b = 180.0$, $\mu_0 = 0.32767$ (crust). And $k = 10^{-0.4}$ for both cases reflecting universal behaviour at high density. n_c , μ_c are the number density and chemical potential where the EoS changes from large n to small n .

3. EOS OF THE NS

The structure of neutron star can be investigated through observations and the modeling of the strongly interacting hadronic matter entirely from the low-density crust to the high-density core inside the star. However, with the absence of accurate and direct first-principles calculation at densities above the nuclear matter saturation (baryon number) density $n_0 \approx 0.16 \text{ fm}^{-3}$, an accurate determination of the state of matter inside NS cores is still unclear. Fortunately, recent observations start offering empirical constraints in both opposing low density and high density limits therefore not only the model-independent approach [5] to the problem has become feasible but also could provide a proper direction for the model-building approach.

3.1. EoS of nuclear matter in low and intermediate density regime

At low density, there is a limitation that comes from the well-studied NS crust region[19] to the density $n_{\text{CET}} \equiv 1.1n_0$, where matter occupies the hadronic-matter phase using chiral effective field theory (CET) which provides the EoS to good precision, currently better than $\pm 24\%$ [20, 21].

For very low density crust, EoS can be found from Table 7 of Ref. [22], it can be fit with the following functions,

$$\begin{aligned} P(\rho) &= \kappa_a \rho^{\Gamma_a} + \kappa_b \rho^{\Gamma_b} + \kappa_c \rho^{\Gamma_c}, \\ &\quad \text{for } 1.32164 \times 10^{-7} < \rho < 87.07, \\ P(\rho) &= \kappa_e \rho^2 + \alpha_e, \quad \text{for } \rho < 1.32164 \times 10^{-7} \end{aligned} \quad (18)$$

where $(\Gamma_a, \Gamma_b, \Gamma_c) = (1.41157, 1.39774, 1.43333)$ and $(\kappa_a, \kappa_b, \kappa_c) = (-0.488954, 0.310732, 0.179472)$, while $(\kappa_e, \alpha_e) = (280.00, -6.0000 \times 10^{-21})$ for the pressure and density expressed in the unit of MeV/fm^3 .

For slightly higher density in the range $87.07 \text{ MeV}/\text{fm}^3 < \rho c^2 < 165.3 \text{ MeV}/\text{fm}^3$ of Table 5 of Ref. [22], the energy density and pressure of the nuclear matter can be expressed as

$$\rho(\bar{n})c^2/T_0 = a_0 \bar{n}^{5/3} + b_0 \bar{n}^2 + c_0 \bar{n}^{\gamma+1}, \quad (19)$$

where $\bar{n} = n/n_0$ and

$$P(\bar{n})/T_0 = \frac{2}{3} n_0 a_1 \bar{n}^{5/3} + n_0 b_1 \bar{n}^2 + \gamma n_0 c_1 \bar{n}^{\gamma+1}, \quad (20)$$

for $T_0 = 36.84 \text{ MeV}$ and $a_0 = 176.209, b_0 = -250.992, c_0 = 100.253$. For the upper limit and the lower limit (the blue dashed lines in Fig. 2), $(a_1, b_1, c_1) = (1.55468, -2.50096, 1.44835)$ and $(1.33832, -2.0337, 1.07001)$ respectively.

For intermediate density, the stiff, intermediate and soft piecewise polytrope extension of the equation of states to higher densities from Ref. [22] each with three exponents Γ_1, Γ_2 and Γ_3 , can be written as follows,

$$\begin{aligned} P(\rho) &= \kappa_1 \rho^{\Gamma_1}, \quad \text{for } \rho_1 \leq \rho \leq \rho_{12}, \\ P(\rho) &= \kappa_2 \rho^{\Gamma_2}, \quad \text{for } \rho_{12} \leq \rho \leq \rho_{23}, \\ P(\rho) &= \kappa_3 \rho^{\Gamma_3}, \quad \text{for } \rho_{23} \leq \rho \leq \rho_{max}. \end{aligned} \quad (21)$$

With mass density $\rho = mn$,

1. the stiff EoS (red dashed line in Fig. 2) has the exponents $(\Gamma_1, \Gamma_2, \Gamma_3) = (4.5, 5.5, 3.0)$ where $(\rho_{12}, \rho_{23}, \rho_{max}) = (1.5\rho_s, 2.0\rho_s, 3.3\rho_s)$ and $(\kappa_1, \kappa_2, \kappa_3) = (11.6687, 51.7666, 2.56345)$.
2. the intermediate EoS (orange dashed line in Fig. 2) has the exponents $(\Gamma_1, \Gamma_2, \Gamma_3) = (4.0, 3.0, 2.5)$ where $(\rho_{12}, \rho_{23}, \rho_{max}) = (3.0\rho_s, 4.5\rho_s, 5.4\rho_s)$ and $(\kappa_1, \kappa_2, \kappa_3) = (2.89711, 1.30607, 1.07402)$.

3. the soft EoS (green dashed line in Fig. 2) has the exponents $(\Gamma_1, \Gamma_2, \Gamma_3) = (1.5, 6.0, 3.0)$ where $(\rho_{12}, \rho_{23}, \rho_{max}) = (2.5\rho_s, 4.0\rho_s, 7.0\rho_s)$ and $(\kappa_1, \kappa_2, \kappa_3) = (0.0321845, 2.63607, 0.572502)$,

when both pressure and density are in GeV/fm^3 and the density scale is $\rho_s = 0.150273 \text{ GeV}/\text{fm}^3$.

Since the mass and moment of inertia of the dense neutron star are mostly determined by the mass in the region $\rho > \rho_s/2$, the cutoff may be applied at $\rho(r = R) = \rho_s/2$ to define radius R of the star. A smaller cutoff will lead to significantly larger radius with larger uncertainty but the mass and moment of inertia relevant to rotational dynamics will remain the same with negligible changes (only $0.1 - 0.7\%$ mass increase) since the density in the extended region is negligibly small.

3.2. EoS of SS model for high density

At high densities inside the NS core, baryons would be tightly compressed, quarks and gluons would be so close together that individual quark and gluon are deconfined from a single baryon and yet the interaction could still be sufficiently strong. The gluons and quarks become deconfined but could still form bound states of multiquark. The multiquarks can possess colour charges in the deconfined phase while keeping the star colour singlet in totality, similar to ionized gas of positive and negative electric charges with total neutrality. In the multiquark model of Ref. [6], the colour charge is quantified by the number fractions of hanging radial strings n_s . For extreme density at relatively moderate temperature, the deconfined phase of quarks and gluons should be in the multiquark phase instead of the pure gas of quarks and gluons where perturbative QCD (pQCD) is applicable.

The multiquark EoS (16),(17) are expressed in dimensionless form. Apart from the colour charge parameter n_s , there is only one parameter we can choose to determine the entire behaviour of the EoS, the energy density scale ϵ_s which will give the physical density and pressure $\rho\epsilon_s, P\epsilon_s$. After choosing ϵ_s , the corresponding distance scale of the SS model is fixed by $r_0 = (G\epsilon_s/c^4)^{-1/2}$.

The pQCD calculation, for the deconfined quarks and gluons of Ref. [23, 24] is also displayed for comparison in Fig. 2.

3.3. Matching of holographic multiquark EoS with low-density nuclear matter EoS

The results, Fig. 1 and 2, of Ref. [5] suggest that there is a double-power-law type EoS interpolating between the high and low density EoS given by pQCD and CET. One such candidate can be found in early work of holographic SS model [7] where the multiquark phase is shown to dominate at large density and moderate temperature. There is only one parameter to be chosen in this model, the energy density scale ϵ_s . By adjusting $\epsilon_s = 23.2037$

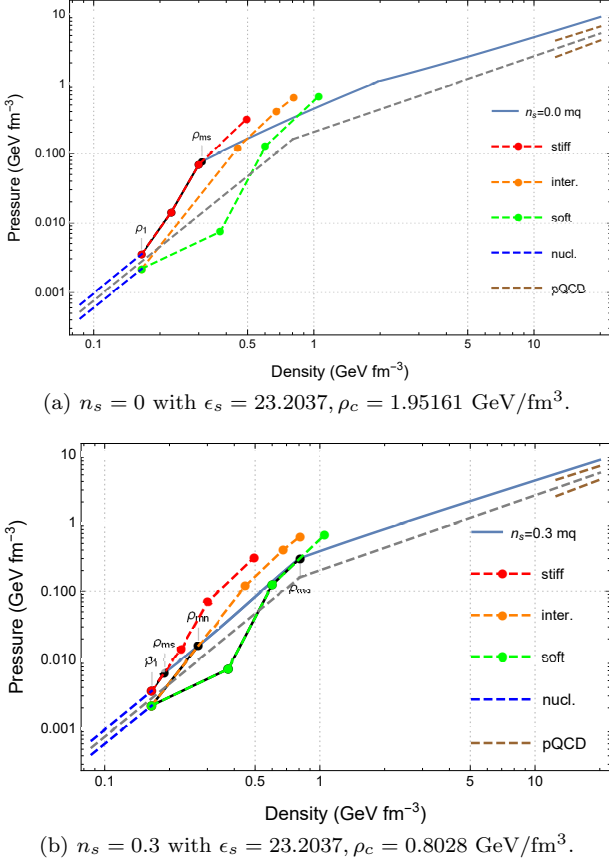


FIG. 2: EoS of multiquark interpolating between nuclear matter and extreme density region

GeV/fm³ to give transition density $\rho_c = 0.8028$ GeV/fm³ as suggested by the turning point of EoS in Fig. 1 of Ref. [5], a good interpolating EoS of $n_s = 0.3$ multiquark matter given by (16), (17) can be achieved as shown in Fig. 2(b). The gray dashed line is the average empirical EoS connecting between pQCD and nuclear phases.

It is remarkable that the EoS of multiquark nuclear matter with $n_s = 0.3$ naturally interpolates between the high and low density. For intermediate densities where piecewise polytropes are used as empirical extension, the EoS of multiquark with $n_s = 0.3$ at low density given by (16) can serve as an excellent average representative of the stiff, intermediate and soft EoS.

4. MR DIAGRAM OF NS WITH MULTIQUARK CORE

The Tolman-Oppenheimer-Volkoff equation [7–9] is used in the consideration of mass profile of the NS,

$$\begin{aligned} \frac{dP}{dr} &= -\frac{(\rho c^2 + P)}{2} \frac{8\pi Pr^3 + 2M(r)}{r(r - 2M(r))}, \\ \frac{dM(r)}{dr} &= 4\pi \rho r^2, \end{aligned} \quad (22)$$

where $M(r)$ is the accumulated mass of the star up to radius r . In determination of the mass-radius diagram shown in Fig. 3, we use the multiquark EoS given in (16), (17) for high density region. As the density and pressure go down within the star and reach transition point with either stiff, intermediate or soft EoS, the new piecewise polytrope EoS (21) is adopted until it reaches the low density region where the EoS given in (20), (19), and (18) will be used subsequently. From Fig. 2, we focus our consideration to 5 scenarios: $n_s = 0.3$ with transition to stiff, intermediate, soft EoS; $n_s = 0$ with transition to stiff EoS; pure $n_s = 0.3$ multiquark. The last scenario is the hypothetical multiquark star with no baryon crust. It is apparent from Fig. 2 that $n_s = 0$ multiquark interpolates worse than $n_s = 0.3$. So just for comparison, we consider only the scenario of the $n_s = 0$ case which would provide the highest possible mass where it is continued with the stiff EoS.

From Fig. 3 for NS containing multiquark core with colour charge fractions $n_s = 0.3$ continuing to intermediate/stiff polytrope extended EoS, the maximum masses are roughly $2.2 - 2.3M_\odot$ with the radii $R \sim 11 - 11.5$ km. For NS containing multiquark core with $n_s = 0.3$ continuing to soft EoS, the maximum mass $\sim 2.1M_\odot$ with radius around 10 km. For star containing multiquark core with $n_s = 0$ (colourless states), the mass could be as large as $2.8M_\odot$ and radii around 14 km. For pure multiquark star with no baryon crust and $n_s = 0.3$, the maximum mass is $\sim 2.3M_\odot$ with radius around 11.5 km.

As shown in Fig. 4, the multiquark core at the maximum masses could have masses and radii in the range $2 - 2.1M_\odot$ and 10 km for $n_s = 0.3$ multiquark continuing to intermediate/stiff EoS and $1.1M_\odot$ and 7 km for $n_s = 0.3$ continuing to soft EoS respectively. For $n_s = 0$ multiquark core continuing to the stiff EoS, the mass and radius of multiquark core is $\sim 1.2 - 1.3M_\odot$ and 9 km. Note that this multiquark core contains both high and low density layers governed by (17) and (16).

Multiquark EoS contains two power-laws governing at high and low density, the corresponding multiquark matter is called the multiquark core and crust in Ref. [7], but to avoid confusion we instead label them with “mqh, mql” respectively in this work. Each region gives different adiabatic indices γ and sound speed c_s as shown in Fig. 5. Interestingly, $\gamma \approx 1$ (2.5) for high (low) density multiquark respectively while $c_s^2 > 1/3$ violating the conformal bound for the high density region and most of the low density region. In the high density region $c_s^2 \simeq 0.426$ for $n_s = 0.3$, this is the value slightly above the conformal bound obeyed by the typical massless free quarks phase. The adiabatic index γ of the high-density multiquark (mqh) is very close to 1 (again the conformal limit of free quarks) while the low-density multiquark (mql) has $\gamma \approx 2.5$, behaving more similar to the hadronic nuclear matter, but with colour charges and deconfined. On the other hand, $n_s = 0$ colourless multiquark at high density has $\gamma \simeq 1.5$, $c_s^2 \lesssim 0.55$.

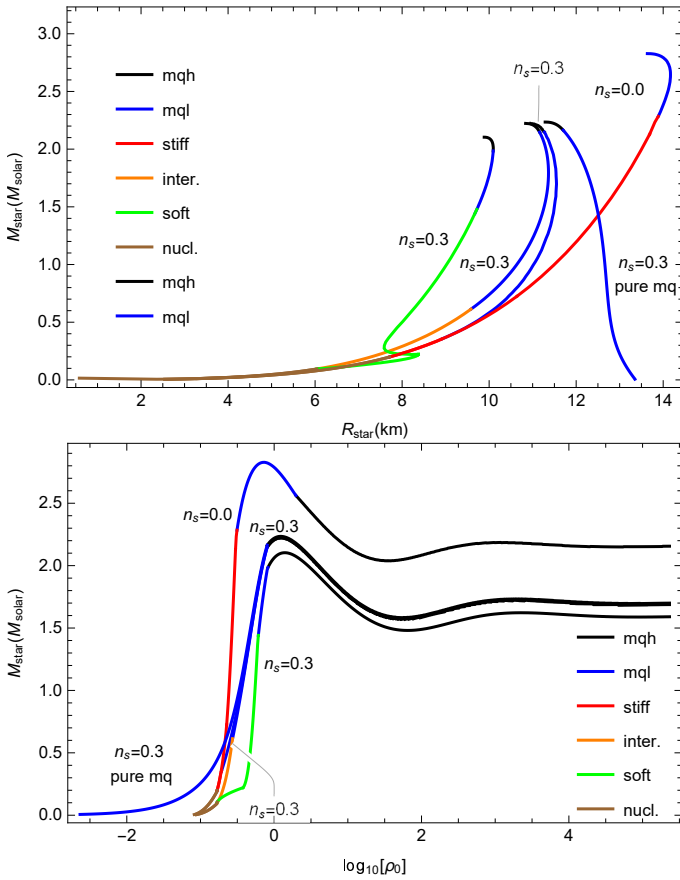


FIG. 3: MR diagram and mass-central density of NS and quark star. The colour label represents the corresponding nuclear phase at the center of the star. Each point corresponds to a star with mass profile consisting of subsequent layers of nuclear phases in order of high to low density: multiquark, polytrope (stiff, intermediate, soft), and CET. The pure hypothetical multiquark star has only multiquark layers.

5. CONCLUSIONS AND DISCUSSIONS

The holographic SS model of multiquark nuclear matter has been applied to the inner core of NS at moderate temperature. The EoS of the multiquark is interpolated between the high density and the low density where the CET is applicable. The energy density scale is fixed once the transition density ρ_c between the power laws in the empirical EoS is chosen. It is found that multiquark with colour-charge fraction $n_s = 0.3$ can interpolate well between the high and low density regions. MR diagram for various scenarios demonstrate that NS with multiquark core can have mass in the range $2.0 - 2.8M_\odot$ and radii $10 - 14$ km.

At higher temperature in the order of trillion Kelvins, the population of multiquarks should become less and the deconfined phase would consist mainly of weakly coupled quarks and gluons. Holographic models including the SS model predict the pressure of this phase to be higher than the multiquark phase. In newly formed NS or ex-

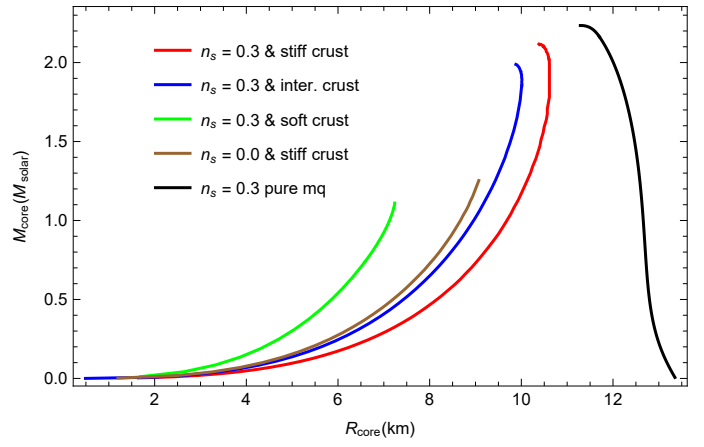


FIG. 4: MR diagram of multiquark core for each curve in Figure 3.

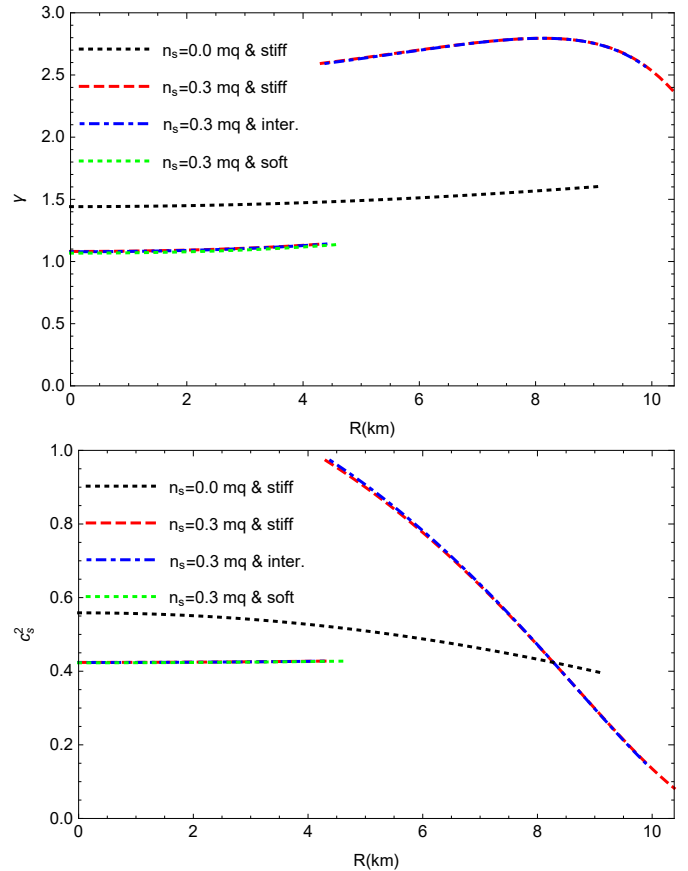


FIG. 5: The adiabatic index $\gamma = \frac{d \ln P}{d \ln \rho}$ and c_s^2 of the multiquark core for each scenario, the multiquark core consists of two regions with high and low density given by (17) and (16).

otic quark star if the core temperature could reach over a trillion Kelvin, it is possible to have this weakly-coupled quarks and gluons in the most inner core follow by multiquark layers resulting in even larger mass of the NS most likely larger than $2M_\odot$. For aged NS with lower temperatures however, we expect only the multiquark phase to

exist in the core. As density decreases with radial distance, the multiquark matter undergoes phase transition into confined baryonic matter or even coexist in mixed phase. For all scenarios that we consider, the NS with multiquark core could exist in a wide range of masses $M > 1.5M_{\odot}$ with radii around $10 - 11.5$ km for $n_s = 0.3$ and $M > 2.3M_{\odot}$ with radii around 14 km for $n_s = 0$. There is a considerable number of observations of NS with masses above $2M_{\odot}$, e.g. Ref. [25–35]. It seems the massive NSs are abundant and our analyses suggest that they likely contain the multiquark cores.

Acknowledgments

P.B. is supported in part by the Thailand Research Fund (TRF), Office of Higher Education Commission (OHEC) and Chulalongkorn University under grant RSA6180002. S.P. is supported in part by the Second Century Fund: C2F PhD Scholarship, Chulalongkorn University.

Appendix A: MR diagram for zero cutoff

In the main text, we use cutoff $\rho_s/2$ to define the radius of the stars. The mass-central density plot in Fig. 3 is insensitive to smaller cutoff, implying that the mass distribution in the extended region is extremely dilute

behaving more like atmosphere of the star consisting of the nuclear matter with EoS given by (18). The maximum masses only increase by $0.1 - 0.7\%$ with zero cutoff. The mass, the moment of inertia, the quadrupole moment of the star thus do not change significantly with smaller cutoff even though the radius increases. For completeness, the mass-radius diagram when the cutoff is zero is presented in Fig. 6.

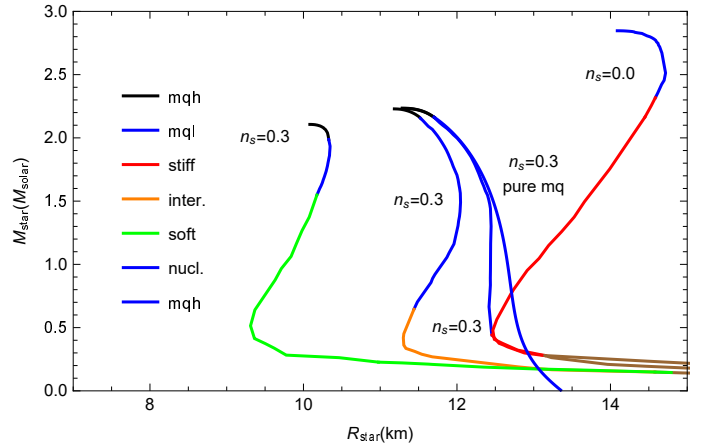


FIG. 6: MR diagram for zero cutoff. The colour label represents the corresponding nuclear phase at the center of the star.

[1] Gyulassy, M., McLerran, L., “New forms of QCD matter discovered at RHIC”, Nucl. Phys. A750, 30–63 (2005).
[2] Andronic, A., Braun-Munzinger, P., Redlich, K. and Stachel, J., “Decoding the phase structure of QCD via particle production at high energy”, Nature561, 321–330 (2018).
[3] Demorest, P. B., Pennucci, T., Ransom, S. M., Roberts, M. S. E. and Hessels, J. W. T. “A two-solar-mass neutron star measured using Shapiro delay.”, Nature467, 1081–1083 (2010).
[4] Antoniadis, J. et al. “A massive pulsar in a compact relativistic binary.”, Science340, 1233232 (2013).
[5] E. Annala, T. Gorda, A. Kurkela, J. Nättälä and A. Vuorinen, “Evidence for quark-matter cores in massive neutron stars,” Nature Phys. (2020) doi:10.1038/s41567-020-0914-9 [arXiv:1903.09121 [astro-ph.HE]].
[6] P. Burikham, A. Chatrabhuti and E. Hirunsirisawat, “Exotic multi-quark states in the deconfined phase from gravity dual models,” JHEP **05** (2009) 006, [arXiv:0811.0243 [hep-ph]].
[7] P. Burikham, E. Hirunsirisawat and S. Pinkanjanarod, “Thermodynamic properties of holographic multiquark and the multiquark star,” JHEP **06** (2010) 040, [arXiv:1003.5470 [hep-ph]].
[8] R.C. Tolman, “Static solutions of Einstein’s field equations for spheres of fluid,” Phys. Rev. **55** (1939) 364.
[9] J.R. Oppenheimer and G.M. Volkoff, “On Massive Neutron Cores,” Phys. Rev. **55** (1939) 374.
[10] R. Aaij *et al.* [LHCb], [arXiv:2006.16957 [hep-ex]].
[11] R. Abbott *et al.* [LIGO Scientific and Virgo], Astrophys. J. **896**, no.2, L44 (2020) doi:10.3847/2041-8213/ab960f [arXiv:2006.12611 [astro-ph.HE]].
[12] Juan M. Maldacena, “Wilson loops in large N field theories,” Phys. Rev. Lett. **80** (1998) 4859–4862, [arXiv:hep-th/9803002].
[13] E. Witten, “Baryons and Branes in Anti-de Sitter Space,” JHEP **07** (1998) 006, [arXiv:hep-th/9805112].
[14] D. J. Gross and H. Ooguri, “Aspects of large N gauge theory dynamics as seen by string theory,” Phys. Rev. D**58** (1998) 106002, [arXiv:hep-th/9805129].
[15] T. Sakai and S. Sugimoto, “Low Energy Hadron Physics in Holographic QCD,” Prog. Theor. Phys. **113** (2005) 843, [arXiv:hep-th/0412141].
[16] T. Sakai and S. Sugimoto, “More on a Holographic Dual of QCD,” Prog. Theor. Phys. **114** (2005) 1083, [arXiv:hep-th/0507073].
[17] P. Burikham and E. Hirunsirisawat, Adv. High Energy Phys. **2011**, 123184 (2011) doi:10.1155/2011/123184
[18] O. Aharony, J. Sonnenschein, S. Yankielowicz, “A holographic model of deconfinement and chiral symmetry restoration”, Ann. Phys. **322** (2007) 1420. arXiv:hep-th/0604161.
[19] Fortin, M. et al., “Neutron star radii and crusts: uncertainties and unified equations of state”, Phys. Rev. C **94**, 035804 (2016).
[20] Gandolfi, S., Illarionov, A. Y., Schmidt, K. E., Pederiva, F., and Fantoni, S. , “Quantum Monte Carlo calculation of the equation of state of neutron matter”, Phys. Rev.

C 79, 054005 (2009).

[21] Tews, I., Krüger, T., Hebeler, K., and Schwenk, “A. Neutron matter at next-to-next-to-next-to-leading order in chiral effective field theory”, *Phys. Rev. Lett.* 110, 032504 (2013).

[22] K. Hebeler et al., “Equation of state and neutron star properties constrained by nuclear physics and observation”, *2013 ApJ* 773 11

[23] Kurkela, A., Romatschke, P., and Vuorinen, A., “Cold quark matter”, *Phys. Rev. D* 81, 105021 (2010).

[24] Gorda, T., Kurkela, A., Romatschke, P., Säppi, M., and Vuorinen, A., “Next-to-next-to-next-to-leading order pressure of cold quark matter: leading logarithm”, *Phys. Rev. Lett.* 121, 202701 (2018).

[25] J. S. Clark, S. P. Goodwin, P. A. Crowther, L. Kaper, M. Fairbairn, N. Langer and C. Brocksopp, *Astron. Astrophys.* **392**, 909-920 (2002) doi:10.1051/0004-6361:20021184 [arXiv:astro-ph/0207334 [astro-ph]].

[26] R. W. Romani, A. V. Filippenko, J. M. Silverman, S. B. Cenko, J. Greiner, A. Rau, J. Elliott and H. J. Pletsch, *Astrophys. J. Lett.* **760**, L36 (2012) doi:10.1088/2041-8205/760/2/L36 [arXiv:1210.6884 [astro-ph.HE]].

[27] R. W. Romani, *Astrophys. J. Lett.* **754**, L25 (2012) doi:10.1088/2041-8205/754/2/L25 [arXiv:1207.1736 [astro-ph.HE]].

[28] M. H. van Kerkwijk, R. Breton and S. R. Kulkarni, *Astrophys. J.* **728**, 95 (2011) doi:10.1088/0004-637X/728/2/95 [arXiv:1009.5427 [astro-ph.HE]].

[29] M. Linares, T. Shahbaz and J. Casares, *Astrophys. J.* **859**, no.1, 54 (2018) doi:10.3847/1538-4357/aabde6 [arXiv:1805.08799 [astro-ph.HE]].

[30] V. Bhalerao, M. H. van Kerkwijk and F. Harrison, *Astrophys. J.* **757**, 10 (2012) doi:10.1088/0004-637X/757/1/10 [arXiv:1207.0008 [astro-ph.SR]].

[31] H. T. Cromartie, E. Fonseca, S. M. Ransom, P. B. Demorest, Z. Arzoumanian, H. Blumer, P. R. Brook, M. E. DeCesar, T. Dolch, J. A. Ellis, R. D. Ferdman, E. C. Ferrara, N. Garver-Daniels, P. A. Gentile, M. L. Jones, M. T. Lam, D. R. Lorimer, R. S. Lynch, M. A. McLaughlin, C. Ng, D. J. Nice, T. T. Pennucci, R. Spiewak, I. H. Stairs, K. Stovall, J. K. Swiggum and W. Zhu, *Nature Astron.* **4**, no.1, 72-76 (2019) doi:10.1038/s41550-019-0880-2 [arXiv:1904.06759 [astro-ph.HE]].

[32] D. J. Nice, E. M. Splaver, I. H. Stairs, O. Loehmer, A. Jessner, M. Kramer and J. M. Cordes, *Astrophys. J.* **634**, 1242-1249 (2005) doi:10.1086/497109 [arXiv:astro-ph/0508050 [astro-ph]].

[33] P. Demorest, T. Pennucci, S. Ransom, M. Roberts and J. Hessels, *Nature* **467**, 1081-1083 (2010) doi:10.1038/nature09466 [arXiv:1010.5788 [astro-ph.HE]].

[34] P. C. C. Freire, *AIP Conf. Proc.* **983**, no.1, 459-463 (2008) doi:10.1063/1.2900274 [arXiv:0712.0024 [astro-ph]].

[35] H. Quaintrell, A. J. Norton, T. D. C. Ash, P. Roche, B. Willems, T. R. Bedding, I. K. Baldry and R. P. Fender, *Astron. Astrophys.* **401**, 313-324 (2003) doi:10.1051/0004-6361:20030120 [arXiv:astro-ph/0301243 [astro-ph]].